Soft Matter

Volume 1 | Number 1 | Jan 2013 | Pages 1–100

Soft Matter

www.rsc.org/softmatter

ROYAL SOCIETY OF CHEMISTRY

ROYAL SOCIETY OF CHEMISTRY

www.rsc.org/softmatter

ARTICLE TYPE   www. rsc.org/xxxxxx | XXXXXXXX

Nonuniform growth and topological defects in the shaping of elastic sheets

Nakul P. Bende, Ryan C. Hayward and Christian D. Santangelo[*]

We demonstrate that shapes with zero Gaussian curvature, except at singularities, produced by the growth-induced buckling of a thin elastic sheet are the same as those produced by the Volterra construction of topological defects in which edges of an intrinsically flat surface are identified. With this connection, we study the problem of choosing an optimal pattern of growth for a prescribed developable surface, finding a fundamental trade-off between optimal design and the accuracy of the resulting shape which can be quantified by the length along which an edge should be identified.

Non-uniform growth processes in elastic sheets have been exploited to create a wide variety of target shapes[1,2]. The underlying concept is that spatially nonuniform growth induces in-plane stresses which are relieved if the sheet buckles[3–5]. In the limit of infinitesimal thickness and free boundaries, the resulting Gaussian curvature is determined entirely by the pattern of growth and whether that growth can be realized physically[6]. Yet we may also produce Gaussian curvature by removing a wedge from a sheet of paper and identifying the newly cut edges, which indeed buckles the sheet into a cone with singular Gaussian curvature at the tip[7,8]. This illustrates a deep relationship between disclinations and Gaussian curvature[9], and has wide-ranging implications in the faceting of viruses[10] and fullerenes[11], shape transitions in protein-coated cell membranes[12], and buckling in graphene[13]. Indeed, the engineering of crystalline defects has been proposed as a means to control shape elastically[14].

It is clear that there must be a relationship between these two processes in the limit of small curvatures: generalizations of the Föppl-von Kàrmàn equations show that defects[9] and nonuniform growth[15] enter the equations in the same manner. Yet the relationship between metric-induced growth and disclinations has not yet been explored in depth, and there is little understanding of more complex patterns of disclinations. In this paper, we will exhibit a mapping between surfaces with only point singularities of Gaussian curvature produced by non-uniform, isotropic growth and by the Volterra construction of disclinations and dislocations[16]. This mapping is beyond geometrical – it is an equivalence between minima of the elastic energy formed with two different processes. Making this relationship explicit, as we have done, has far reaching consequences: not only can we exploit the mapping to predict
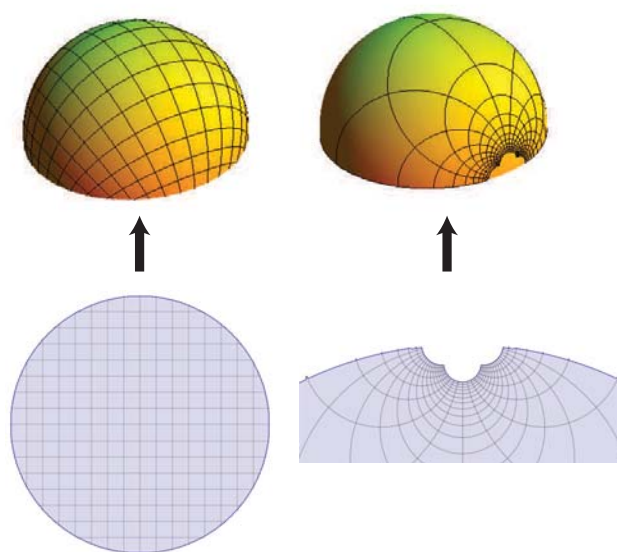
Fig. 1 (color online) There are many ways of associating a conformal coordinate system, appropriate to an isotropic growth pattern, to a shape. Two domains are shown, both of which can be mapped to the same sphere with different growth patterns. The degree of growth required is related to the area between the coordinate lines. These two domains are related by the mapping $w = g(z) = z/(1-z)$.

University of Massachusetts, Amherst, 666 N. Pleasant St., Amherst, MA, USA. E-mail: csantang@physics.umass.edu

shapes resulting from nonuniform growth using only paper, scissors and adhesive, inverting the mapping allows us to find growth patterns that can be more optimally implemented experimentally. These results also give a better sense of what the limits are of growth-induced shapes and, indeed, we identify two antagonistic trade-offs occurring in the design of realistic structures.

Isotropic growth can be described in terms of a prescribed metric, given by $ds^2 = \Omega(x,y)(dx^2 + dy^2)$, where $\Omega(x,y)$ gives a multiplicative increase in area[4]. The function $\Omega(x,y)$ can be controlled, for example, through the local monomer[1] or cross link density[2] of a polymer gel that, subsequently, swells in a solvent. The resulting equilibrium shape is then described by a solution to a set of covariant equations (see, for example,[17–19]), the precise form of which is not needed in our analysis here. Covariance of the equilibrium equations implies the simple result that the solutions are invariant with respect to changing how points on the surface are labeled. Therefore, if we introduce a new coordinate system (u,v) such that the growth is described by the metric $ds^2 = \tilde{\Omega}(u,v)[du^2 + dv^2]$, the physical shape of the solution remains invariant. Starting from the same buckled surface, then, we can produce two different flat domains by "ungrowing" according to either $1/\Omega(x,y)$ or $1/\tilde{\Omega}(u,v)$ (Fig. 1). Thus, we arrive at our first mathematical result: the (u,v) domain and growth pattern $\tilde{\Omega}(u,v)$ and the (x,y) domain with growth pattern $\Omega(x,y)$ yield the same three-dimensional solution to the equilibrium equations (Fig. 1).

For isotropic growth, the mapping between (x,y) and (u,v) is most compactly expressed using complex coordinates $z = x + iy$ and $w = u + iv$. In a domain of the complex w−plane, $ds^2 = 2\Omega(w,\overline{w})dwd\overline{w}$. Similarly, we define an analytic function $g(z)$ such that $w = g(z)$ maps a domain in the z−plane to one in the w−plane. It follows that the prescribed metric is $ds^2 = 2\Omega[g(z),\overline{g(z)}]|\partial g(z)|^2 dzd\overline{z}$, where $\partial \equiv (\partial_x - i\partial_y)/2$. Consequently, a domain in the z−plane with isotropic growth

$$\Omega[g(z),\overline{g(z)}]|\partial g(z)|^2 \qquad (1)$$

will produce the same shape as the domain $g(z)$ in the w−plane with isotropic growth $\Omega[w,\overline{w}]$.

In what follows, let us restrict ourselves to isotropic growth processes resulting in surfaces with zero Gaussian curvature, K, except at isolated singularities. According to Gauss' *theorema egregium*, one has

$$\nabla^2 \ln\Omega = -2K\Omega = -2\sum_i K_i \delta^2(\mathbf{x} - \mathbf{x}_i)\Omega(\mathbf{x}_i), \qquad (2)$$

so that the total Gaussian curvature of the surface is $\int dA\, K = \int d^2x\, \Omega(\mathbf{x}_i)K = \sum_i K_i$. Thus, we obtain the metric

$$\Omega(z,\overline{z}) = |e^{h(z)}|\prod_i |z - z_i|^{-K_i/\pi}, \qquad (3)$$
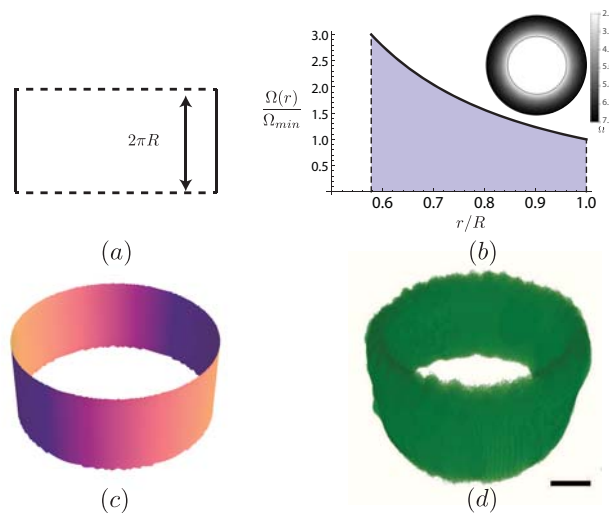
(a)

(b)

(c)

(d)

Fig. 2 (color online) (a) A domain with two opposite sides identified (dashed lines) rolls up to form a cylinder. (b) An annular domain with metric $\Omega = (R/r)^2$ also buckles into a cylinder (inset: the corresponding growth pattern, where Ω is areal swelling ratio). (c) This growth pattern has been tested by numerical minimization of a bead and spring model and (d) can also be seen in 3-d reconstructed images from experiments using halftone gel lithography (scale bar: 200 μm).

where $h(z)$ is an arbitrary, analytic function.

To proceed, start with a domain in the w−plane having metric, $ds^2 = 2dwd\overline{w} = 2|\partial g(z)|^2 dzd\overline{z}$. Thus,

$$\partial g(z) = e^{h(z)/2}\prod_i (z - z_i)^{-K_i/(2\pi)}, \qquad (4)$$

defines a mapping $g(z)$ from a domain in the w−plane with $\Omega(w,\overline{w}) = 1$ to a domain in the z−plane with metric given by Eq. (3). This result, in combination with the general covariance of the elastic equations implies that a pattern of growth, corresponding to a surface with $K = 0$ except at distinct singularities, buckles into the same shape as a domain with no growth at all. As we will see below, the correspondence requires us to identify some of the boundaries in the w−plane, thereby restoring the Gaussian curvature singularities that drive buckling.

The simplest example with which to illustrate the equivalence is the growth pattern, $\Omega(z,\overline{z}) = R^2/|z|^2$, defined on an annulus of inner radius r_0. The mapping to the w−plane is given by (Fig. 2),

$$g(z) = \int dz\, \frac{R}{z} = R\ln(z/R). \qquad (5)$$

Since the logarithm is not single-valued, one must define a branch cut on the complex plane across which $g(z)$ will be discontinuous. One might choose, for example, a branch cut

along the positive real axis. Setting $z = re^{i\theta}$ with $0 \le \theta < 2\pi$ then implies

$$g(re^{i\theta}) = R\ln(r/R) + iR\theta. \qquad (6)$$

Therefore, the region just above the positive real axis is mapped to the real axis in the w−plane while the line just below the positive real axis is mapped to the line $x + i2\pi R$. Since these two regions are connected across the positive real axis in the z−plane, the mapping requires us to identify the real axis with the line at $2\pi iR$ in the w−plane. This, of course, is a standard construction for a cylinder.

To confirm this, we performed simulations of a film described by a system of points connected by springs. The growth pattern is encoded by choosing equilibrium spring lengths according to $\Omega(z, \bar{z})$, as described in Refs.[4,20]. The resulting shape is, indeed, cylindrical and, even though it was produced from an annulus with a very different growth pattern near the inner and outer boundary, the result is nevertheless reflection symmetric (Fig. 2c). Even thick cylinders, which show a gentle flaring at both edges, maintain the symmetry one would expect from the mathematical equivalence encoded in Eq. (6).

To realize the mapping of topological defects to metrics with singularities in Gaussian curvature experimentally, we use halftone gel lithography (described in detail elsewhere[2]) to pattern poly(N-isopropyl acrylamide-co-acrylic acid-co-benzophenone acrylamide-co-fluorescein acrylate) (PNipam) films of thickness $\sim 10\mu m$ and lateral dimensions of 300 – 700 μm. Halftoning relies on the bending elasticity of the finite-thickness sheet to smooth out the sharp changes in swelling defined by highly crosslinked dots in a lightly crosslinked matrix, yielding effectively smooth variations in swelling. Target metrics were discretized into a pattern of dots on a hexagonal lattice using MATLAB (Mathworks), and converted to AutoCAD (Autodesk) format for printing (Front Range Photomasks) as a chrome on glass mask with a resolution of $3\mu m$. Gel sheets were prepared by drop-casting a polymer solution in chloroform on a sacrificial polyacrylic acid film. For each object, two photo-masks were used to define regions with different degrees of crosslinking using an inverted optical microscope (Zeiss Axiovert 200) and a fluorescence excitation lamp (EXFO X-Cite 120 Q) as a UV source. The patterned film was next developed by Ethanol: water mixture (1:2 by volume) and released by swelling in phosphate buffered saline (PBS) solution (containing 1 mM NaCl and 1 mM phosphate buffer, pH 7.2). The shape of the swelled gel film was then characterized using a laser scanning confocal fluorescence microscope (Zeiss LSM 510 Meta) using ImageJ for 3D reconstruction. Fig. 2d shows a cylindrical film produced from an initially flat annulus, using halftone gel lithography to pattern the swelling of a photo-crosslinkable polymer film.
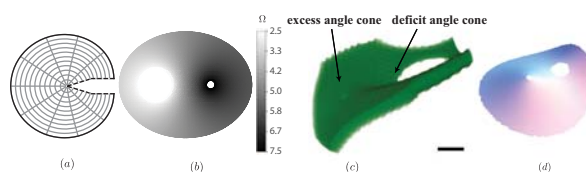

Fig. 3 (color online) (a) Domain in the w−plane for a dipole of strength $K|z_0|^2/(2\pi) = -10^{-1}$. (b) Resulting growth pattern in the z−domain. (c) The physical dipole formed by the corresponding growth pattern using halftone gel lithography (scale bar: 200 μm) and (d) numerical minimization. Only one of the two possible dipolar geometries identified in[8] is seen.

Eq. (4) provides us with a connection between Gaussian curvature and the Volterra construction of a disclination formed by removing a wedge of fixed angle. To make this connection explicit, consider an annulus with $\Omega = |z/R|^{-K/\pi}$, which buckles into a cone[2]. This shape is equivalent to a domain with no growth under the mapping

$$g(z) = \frac{(z/R)^{1-K/(2\pi)}}{1 - K/(2\pi)}. \qquad (7)$$

Again, there is a branch point at the origin and infinity; choosing the branch cut along the positive real axis, we find that we must identify the two radial lines across a wedge of angle K. More generally, we see that singularities of Gaussian curvature can naturally be identified with a Schwarz-Christoffel-like transformation

$$g(z) = \int dz \prod_i (z - z_i)^{-(\bar{\theta}_i - \theta_i)/(\pi + \bar{\theta}_i)} \qquad (8)$$

where a wedge of angle θ becomes one of angle $\bar{\theta}$. When $\bar{\theta} = \pi$ we obtain the traditional Schwarz-Christoffel transformation; in our correspondence, however, we require $\bar{\theta} = 0$.

A pair of oppositely-charged singularities, corresponding to two opposite disclinations, can be formed from the growth pattern $\Omega(z, \bar{z}) = |z - z_0|^{-K/\pi}|z + z_0|^{K/\pi}$. The mapping $\partial g(z) = (z - z_0)^{-K/(2\pi)}(z + z_0)^{K/(2\pi)}$ has three branch points: z_0, $-z_0$, and ∞. Thus, we must draw branch cuts that go through all three of these branch points to prevent the mapping from being multivalued. We can accommodate this with two branch cuts: from z_0 to infinity and $-z_0$ to infinity; thus, we come to the intuitive conclusion that the resulting shape requires us to remove a wedge of angle K from one singularity and add a wedge of angle K to the other. The shapes of such structures have been studied elsewhere[8].

Yet, in a 2D crystal a pair of opposite disclinations corresponds to a dislocation in which a row of atoms is removed. And indeed there is another way to draw branch cuts through the branch points at $\pm z_0$ and ∞: consider choosing a single branch cut from $-z_0$, passing through z_0 and continuing to infinity. This shape requires only one cut which, as seen in Fig.

3(a) requires only the removal of material. Indeed, far from the singularities, the resulting branch cut appears to be equivalent to the removal of a constant width of material, exactly the way an edge dislocation requires the removal of a row of atoms from a 2D crystal. To see this more clearly, we can study the far-field limit by taking $z_0 \to 0$ while $K|z_0|$ simultaneously remains constant. We find $g(z) = z - (z_0 K/\pi) \ln(z/|z_0|)$. Thus two radial lines on the $z-$plane are mapped to horizontal lines in the $w-$plane that are separated by $g(re^{i2\pi}) - g(r) = i2K|z_0|/\pi$. We can interpret this gap as a dislocation with Burger's vector $i2K|z_0|/\pi$ (Fig. 3). Continuing in this manner, a pair of dislocations can be formed with only an internal branch cut, which forces us to remove material from the interior of a domain.

Finally, we discuss how to produce the inverse mapping from a flat domain to a growth pattern (Fig. 4a). As a concrete example, we consider forming a tetrahedron by folding an equilateral triangle. The growth pattern is described by

$$\Omega(z,\bar{z}) = \Omega_0 |e^{h(z)}|^2 |z^3 - R^3|^{-1}. \tag{9}$$

As there are many growth patterns associated the choice of $h(z)$ and Ω_0, we require some criteria to select among them. For convenience, we set $\Omega_0 = 1$.

To set $h(z)$, note that the local, areal growth, Ω, obtained in any experiment must be bounded between $\Omega_{min} \le \Omega \le \Omega_{max}$. For $K = 0$ surfaces, such as those we are considering, the cores of each singularity can never be accommodated in a finite range of growth and, so, those cores must be excised. Since these cores represent the smallest and largest swelling in any growth pattern associated with Eq. (3), we can formulate our search for an optimal growth pattern to be one that minimizes the area that must be excised around the singularities.

If we naively set $h(z) = 0$, $\Omega(z,\bar{z})$ decreases to zero as $|z|$ becomes large. This immediately suggests the use of virtual singularities of opposite charge just outside the boundary of the domain, so that $\Omega(z,\bar{z}) \to 1$ as $|z| \to \infty$. The closer we are able to place these virtual singularities, the more uniform the growth will be. We proceed with the ansatz

$$|e^{h(z)}|^2 = |z^3 - D^3|^{-1}, \tag{10}$$

where $D > R$ is chosen outside of the material domain. The closer D is to R, the more uniform $\Omega(z,\bar{z})$ will be away from the vicinity of the singularities. The associated mapping is

$$\partial g(z) = \left(\frac{z^3 - D^3}{z^3 - R^3} \right)^{1/2}. \tag{11}$$

From Eq. (8), we identify each singularity with a wedge of deficit angle π, consistent with identifying the two halves of each side of the triangle about its midpoint. With the virtual singularities, however, the entire side is not identified. Indeed,
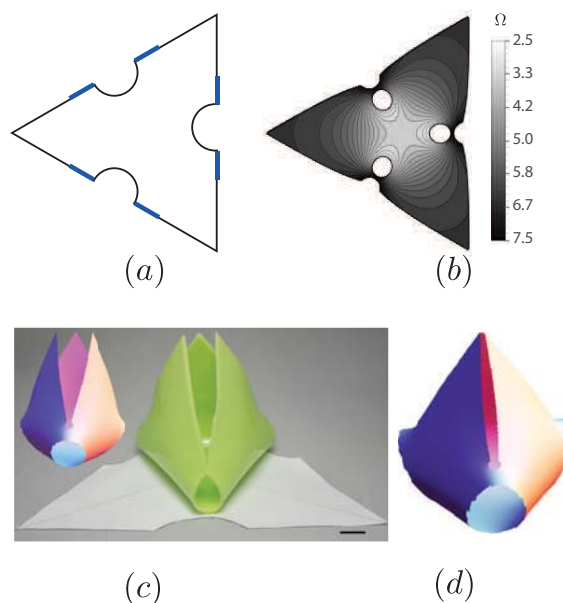

Fig. 4 (color online) (a) Fold pattern for a tetrahedron with singularities removed. We only Identify segments of the sides of length L, which indicated with thick, blue lines. (b) The growth pattern and domain corresponding to (a) for $B/R = D/R = 1.75$. The holes and boundary are chosen so that, $\Omega_{max}/\Omega_{min} = 3$ to correspond with our experimental system. (c) Results of numerical minimization of (b) for a tetrahedron of thickness $0.08R$ (inset) and result of folding (a) in poly(vinyl siloxane). (scale bar: 10mm) (d) On the other hand, numerical minimization in which the each of the three positive singularities have Gaussian curvature 1.3π closes comparatively well.

consider the radial length L between the boundary of the core of the singularity and the outer boundary of Fig. (4b) in the sheet after it has grown to its final buckled configuration. Eq. (9) gives

$$L = R \int_1^{B/R} dx \, \frac{|x^3 - (D/R)^3|}{|x^3 - 1|}. \tag{12}$$

This length L must agree with the length of side in Fig. 4a to be identified. In particular, these lengths are identical because the $w-$plane does not grow at all. This has the propensity to alter the resulting shape somewhat from a completely closed tetrahedron when the thickness is finite (Fig. 4c). Thus, Eq. (12) identifies one essential trade-off: we can make the tetrahedron growth pattern arbitrarily uniform by taking D and $B \to R$ while simultaneously keeping the image singularities outside the boundary. However, we do this at the expense of shortening L, the length of side that is identified in Fig. 4(a).

Beyond this, there is a second trade-off related to the resolution necessary to encode the growth pattern. The maximum

growth occurs on the boundary of the positive Gaussian curvature singularities and the minimum near the virtual singularities. Therefore, the closer a virtual singularity is to a real singularity, the more rapid the change in growth pattern between them. We expect, therefore, that even though a more uniform pattern overall can be achieved by introducing virtual singularities, the region between the singularities and defects must still be accurately represented. Mathematically, we can compute how quickly distance from the singularity at $z = R$ changes as a function of Ω,

$$\frac{dx}{d\Omega} = \frac{D^3 - R^3}{3[(\Omega - 1)^4 (D^3 - \Omega R^3)^2]^{1/3}}. \quad (13)$$

Thus $d\Omega/dx \to \infty$ as $D \to R$. How to put a bound on $d\Omega/dx$ clearly depends on details of a material system, but it is clear that the closer D is to R, the more detailed the growth pattern must be near the boundaries of the sample. This suggests that, at least generically, the resolution to which the metric can be programmed must be balanced with the range of swelling available.

To corroborate our theoretical results, we have simulated the growth pattern in Eq. (11) with $D/R = 1.75$ and boundary $B = D$ (Fig. 4c). The tetrahedron does not close. To corroborate this shape, we also folded a tetrahedron from a thin elastic sheet of poly(vinyl siloxane) (Elite Double 32, Zhermack) using the pattern in Fig. 4a. Attaching the relevant corners with narrow strips of silicone adhesive (ARclad IS-8026, Adhesives Research, Inc.) results in a remarkably similar open tetrahedron (Fig. 4c, inset). One way to close the tetrahedron would be to use a larger range of growth, which would allow us to develop shapes equivalent to identifying a larger length along the boundaries of Fig. 4a. Alternatively, increasing the Gaussian curvature at each of the three singularities to $\approx 1.3\pi$ does result in an imperfectly closed tetrahedron (Fig. 4d).

Even though our analysis only applies, strictly speaking, to surfaces with zero Gaussian curvature almost everywhere, we still believe that the results lend some insight into the optimal design of more general shapes by isotropic growth. In particular, one could imagine approximating a smooth surface using only singularities of Gaussian curvature, much as smooth charge densities approximate discrete charges in electrodynamics. Moreover, our notion of using virtual singularities corresponds with Chebyshev's principle, which states that optimal growth patterns (those having the smallest variation of $\ln \Omega$) also have constant Ω on their boundary[21]. This result can also be understood in terms of an electrostatics analogy: $\ln \Omega$ is analogous to the electric potential, and the boundaries act as conductors. Thus the charge density on the boundary adjusts to the presence of the Gaussian curvature within to minimize the total "electric field."

In summary, we have demonstrated a mapping between the buckling of developable surfaces due to nonuniform growth and the buckling of elastic sheets with a prescribed configuration of Volterra defects. This mapping provides new insights into the trade-offs between the growth pattern and the resulting shape: though there are many potential growth patterns corresponding to the same Gaussian curvature, and indeed ones with a very small range of growth are possible, the ones with largest range of growth will produce better approximations to the desired shape.

References

1 Y. Klein, E. Efrati and E. Sharon, *Science*, 2007, **315**, 1116.
2 J. Kim, J. Hanna, M. Byun, C. Santangelo and R. Hayward, *Science*, 2012, **335**, 1201.
3 E. Sharon, B. Roman, M. Marder and H. Swinney, *Nature*, 2002, **419**, 579.
4 M. Marder and N. Papanicolaou, *J. Stat. Phys.*, 2006, **125**, 1069.
5 J. Dervaux and M. B. Amar, *Phys. Rev. Lett.*, 2008, **101**, 068101.
6 M. Lewicka, L. Mahadevan and R. Pakzad, *Proc. R. Soc. A*, 2010, **467**, 402.
7 M. Müller, M. B. Amar and J. Guven, *Phys. Rev. Lett.*, 2008, **101**, 156104.
8 J. Guven, J. A. Hanna and M. M. O. Kahraman, *Eur. Phys. J. E*, 2013, **36**, 106.
9 H. Seung and D. Nelson, *Phys. Rev. A*, 1988, **38**, 1005.
10 T. Nguyen, R. Bruinsma and W. Gelbart, *Phys. Rev. E*, 2005, **72**, 051923.
11 T. Witten and H. Li, *Europhys. Lett.*, 1993, **23**, 51.
12 R. Mashl and R. Bruinsma, *Biophys. J.*, 1998, **74**, 2862.
13 I. Ovid'ko, *Rev. Adv. Mat. Sci.*, 2012, **32**, 1.
14 E. Yong, D. Nelson and L. Mahadevan, *Phys. Rev. Lett.*, 2013, **111**, 177801.
15 Liang and L. Mahadevan, *Proc. Nat. Acad. Sci.*, 2009, **106**, 22049.
16 V. Volterra, *Ann. Scient. Ec. Norm. Sup. (Paris)*, 1907, **24**, 401.
17 J. Guven and M. Müller, *J. Phys. A*, 2008, **41**, 055203.
18 E. Efrati, E. Sharon and R. Kupferman, *J. Mech. Phys. Sol.*, 2009, **57**, 762.
19 M. Dias, J. Hanna and C. Santangelo, *Phys. Rev. E*, 2011, **84**, 036603.
20 B. Chen and C. Santangelo, *Phys. Rev. E*, 2010, **82**, 056601.
21 D. Grave, *Crelle J.*, 1911, **140**, 247.